Theoretical Investigations of Real Gas Effects in Cryogenic Wind Tunnels

Bernhard Wagner*
Technische Hochschule Darmstadt, Federal Republic of Germany
and
Wolfgang Schmidt†
Dornier GmbH Friedrichshafen, Federal Republic of Germany

Real gas effects in cryogenic nitrogen flows have been calculated using the Beattie-Bridgeman equation of state. The investigations include Prandtl-Meyer expansions, oblique shocks, transonic small perturbation theory, transonic flow past a NACA 0012 aerofoil, and shock-wave/boundary-layer interaction. The last two cases mentioned have been treated with the aid of finite volume techniques. The results show som noticeable deviations from the behavior of an ideal gas, not only at cryogenic conditions but also at normal temperatures and high pressures. Within the operating range of cryogenic wind tunnels the deviations remain very small; only the friction coefficient exhibits a considerable amount of systematic variation.

I. Introduction

THE past has shown for many problems in aircraft aerodynamics the importance of testing in wind tunnels at the same Reynolds numbers as would be obtained in free flight. The great interest in transonic flight, therefore, leads to the development of cryogenic wind tunnels.[1]

These tunnels operate at temperatures close to the liquefaction boundary of the test gas; both the decrease in viscosity and the increase in density result in a large increase in Reynolds number. From the decrease in the speed of sound follows a reduction of the velocity at constant Mach number which counteracts the viscosity and density effects, but the decrease of the velocity also causes a favorable reduction of drive power. Thus, in the U.S. as well as in Europe, the cryogenic concept is preferred for high-Reynolds-number transonic wind tunnels planned for the future.

However, there is some doubt if the data gained from such tunnels can be transferred to the full-scale aircraft within reasonable accuracy or if additional parameters have to be considered due to real gas effects or other changes in the gas properties. Cryogenic nitrogen has been shown by NASA to be an acceptable test gas,[2] but this statement is theoretically based on isentropic expansion and normal shock calculations only. The present study, therefore, aims to look into the theoretical evaluation of such effects for more complicated flows in order to predict experimental error sources.

All real gas results shown are strictly valid only for cryogenic nitrogen. The results for air will differ only by a small amount from those for nitrogen. The pressures chosen for the calculations generally correspond to the pressure range of the U.S. National Transonic Facility (stagnation pressure $p_t \leq 9$ bar) and also include the range of the planned European Transonic Wind Tunnel ($p_t \leq 5$ bar). A few results beyond this range (Figs. 2 and 4) are included to show that the order of magnitude for the real gas effects does not increase when the temperature is reduced at constant pressure. Hence, real gas effects can be expected to decrease mostly by using cryogenic tunnels, since the pressures may be essentially reduced compared with conventional tunnels for the same Reynolds number.

Presented as Paper 77-669 at the AIAA 10th Fluid and Plasma Dynamics Conference, Albuquerque, N. Mex., June 27-29, 1977; submitted Aug. 5, 1977; revision received Jan. 24, 1978.

Index categories: Aerodynamics; Testing, Flight and Ground; Computational Methods.

*Dozent, Institut für Flugtechnik.
†Head, Theoretical Aerodynamics Group. Member AIAA.

II. Thermodynamics

Real gas effects are described using the thermal equation of state given by Beattie-Bridgeman[3] for pressure p as a function of density ρ and temperature T

$$p=\rho RT[1-(c\rho/T^3)][1+B_0\rho(1-b\rho)]-A_0\rho^2(1-a\rho) \quad (1)$$

which includes the empirical constants A_0, B_0, a, b, c describing real gas behavior. Table 1 contains the constants for nitrogen and air assuming p in N/m^2, ρ in kg/m^3, and T in K. In addition, a caloric equation of state is needed, i.e., an equation for the internal energy e. Similar to the procedure for the enthalpy h shown in Ref. 4, such an equation can be derived from thermodynamics. From

$$de=T\,ds-p\,dv \quad (2)$$

with entropy s and specific volume v we get, expressing the total differential ds in terms of differentials in T and v,

$$de=T\left(\frac{\partial s}{\partial T}\right)_v dT+\left[T\left(\frac{\partial s}{\partial v}\right)_T-p\right]dv \quad (3)$$

Equation (2) for constant volume and the requirement that second-order mixed derivatives of the free energy f be equal[5] lead to

$$\left(\frac{\partial e}{\partial T}\right)_v=c_v=T\left(\frac{\partial s}{\partial T}\right)_v \quad (4a)$$

$$\left(\frac{\partial s}{\partial v}\right)_T=\left(\frac{\partial p}{\partial T}\right)_v \quad (4b)$$

With the aid of these equations, the entropy can be eliminated from Eq. (3) using $\rho=1/v$

$$de=c_v dT-\left[T\left(\frac{\partial p}{\partial T}\right)_\rho-p\right]\frac{d\rho}{\rho^2} \quad (5)$$

It should be kept in mind that for a real gas, c_v as a derivative of the internal energy [see Eq. (4a)] still depends on ρ and T in

Table 1 Constants for the Beattie-Bridgeman equation

	Nitrogen	Air
R	296.813	287.11
A_0	173.6	157.2
B_0	1.8013×10^{-3}	1.5922×10^{-3}
a	9.342×10^{-4}	6.668×10^{-4}
b	-2.467×10^{-4}	-3.802×10^{-4}
c	1499	1499

an a priori unknown manner. But since e is a variable of state, the integral over Eq. (5) does not depend on the path of integration and this path can be chosen arbitrarily. We integrate first along the temperature at $\rho_0=0$ and assume that, in this range, the gas behaves like an ideal one and c_v is constant. Choosing $T_0=0$ and $e_0=0$ as integration constants yields

$$e=c_{v_{id}}T-\int_0^\rho\left[T\left(\frac{\partial p}{\partial T}\right)_\rho-p\right]\frac{\mathrm{d}\rho}{\rho^2} \tag{6}$$

The internal energy can be explicitly calculated as a function of ρ and T if Eq. (1) is introduced. The resulting equation for the enthalpy h gives

$$h=e+p/\rho=e(\rho,T)+(1/\rho)p(\rho,T) \tag{7}$$

Furthermore, the entropy often has to be known. Combining Eqs. (2) (5), we get

$$\mathrm{d}s=c_v\frac{\mathrm{d}T}{T}+\left(\frac{\partial p}{\partial T}\right)_v\mathrm{d}v \tag{8}$$

The integral over Eq. (8) again is independent of the path of integration and one can take

$$s-s_0=\int_{T_0}^{T}c_v(T,\rho_0)\,\mathrm{d}T-\int_{\rho_0}^{\rho}\left(\frac{\partial p}{\partial T}\right)_\rho\frac{\partial\rho}{\rho^2} \tag{9}$$

Because of the common logarithmic singularities in the explicit expression for s, one should not use $T_0=\rho_0=0$ as a reference point. Instead, another arbitrary point is chosen as in Jacobsen and Stewart.[6]

Using the set of basic equations (1, 6, 7, and 9), each thermodynamic property can be evaluated for two others given. Only the four properties represented by those four equations can be calculated directly; the rest must be computed by means of an iterative procedure. Derivatives of the basic properties with respect to ρ or T, T and ρ, respectively, being constant, can be derived easily. But other derivatives are also quite important, for example,

$$c_p=\left(\frac{\partial h}{\partial T}\right)_p=T\left(\frac{\partial s}{\partial T}\right)_p \tag{10}$$

Assuming $s=s(T,v)$ and $v=v(T,p)$ yields, using the corresponding total differentials,[5]

$$\left(\frac{\partial s}{\partial T}\right)_p=\left(\frac{\partial s}{\partial T}\right)_v+\left(\frac{\partial s}{\partial v}\right)_T\left(\frac{\partial v}{\partial T}\right)_p$$

Knowing the entropy derivatives from Eqs. (4) and using $p=p(T,v)$ leads to

$$c_p=c_v+\frac{T}{\rho^2}\left(\frac{\partial p}{\partial T}\right)_\rho^2\Big/\left(\frac{\partial p}{\partial\rho}\right)_T \tag{11}$$

Again, all derivatives can be taken directly from Eqs. (1-6). In a similar way, convenient formula can be derived for the speed of sound in real gases[7]

$$a^2=\left(\frac{\partial p}{\partial\rho}\right)_s=\frac{c_p}{c_v}\left(\frac{\partial p}{\partial\rho}\right)_T \tag{12}$$

Figure 1a shows the density deviations for the real gas equation (1) from the thermal equation of state for an ideal gas with $\gamma=1.4$. On approaching the saturation boundary, quite large differences occur. In a similar manner, Fig. 1b presents the deviation in speed of sound. Again, close to saturation the deviations become quite large. The deviations, calculated by using Eq. (1), are also compared in Fig. 1 at $p=10$ bar and $p=2$ bar with more exact data from Ref. 6. The agreement is shown to be excellent, proving that Eq. (1) can be used for the present study. As far as Fig. 1b is concerned, it should be kept in mind that the data from Ref. 6 show some scatter due to round-off errors in the speed of sound values.

III. Basic Nonlinear Supersonic Flows

Prandtl-Meyer Expansions

The change in velocity V and streamline angle δ due to a Mach wave is estimated from momentum balances[5]

$$\mathrm{d}\delta=\pm\sqrt{M^2-1}\frac{\mathrm{d}V}{V}=\pm\frac{1}{2}\sqrt{V^2/a^2-1}\frac{\mathrm{d}V^2}{V^2} \tag{13}$$

M being the local Mach number. For adiabatic flows, conservation of energy gives

$$h(\rho,T)+(V^2/2)=\text{const}=h_{\text{total}} \tag{14}$$

In addition, the Prandtl-Meyer flow is isentropic by definition

$$s(\rho,T)=\text{const}=s_\infty \tag{15}$$

The stagnation values for s and h [i.e., the constants in Eqs. (14) and (15)] being given, the thermodynamic properties ρ and T for each value of V can be iteratively calculated by means of Eqs. (7) and (9). Then the speed of sound can be computed from Eq. (12), and Eq. (13) can be numerically stepwise integrated. The expansions will be limited by the saturation boundary.

Oblique Shocks

For shocks in a real gas, the conservation laws for mass, momentum, and energy are valid in the usual form. These equations, in combination with the thermodynamic equations of state for a real gas, describe the change of flow properties across a shock wave. It is possible to get a relation connecting enthalpies, pressures, and densities across the shock by elimination of the velocity,[5] but it is impossible to eliminate pressure and density from the set of equations, due to the complex thermodynamic relations for real gases. Therefore, the set of equations has been solved by means of an iterative procedure.

Results

Figure 2 shows some results for Prandtl-Meyer expansions with the same initial Mach number $M_\infty=1$ but different initial pressure and temperature. The conditions of the high-pressure cryogenic case ($p_\infty=10$ bar, $T_\infty=120$ K) are beyond the operating range of planned cryogenic wind tunnels, and the results are only shown for comparison of pressure effects at different temperatures. According to Fig. 2a, the density and pressure deviations seem not to be systematically correlated. In some regions the pressure deviations are larger; in others, the density deviations are larger; sometimes they even have different signs. But all deviations are within 0.5%. Anyway, it should be mentioned that for small initial

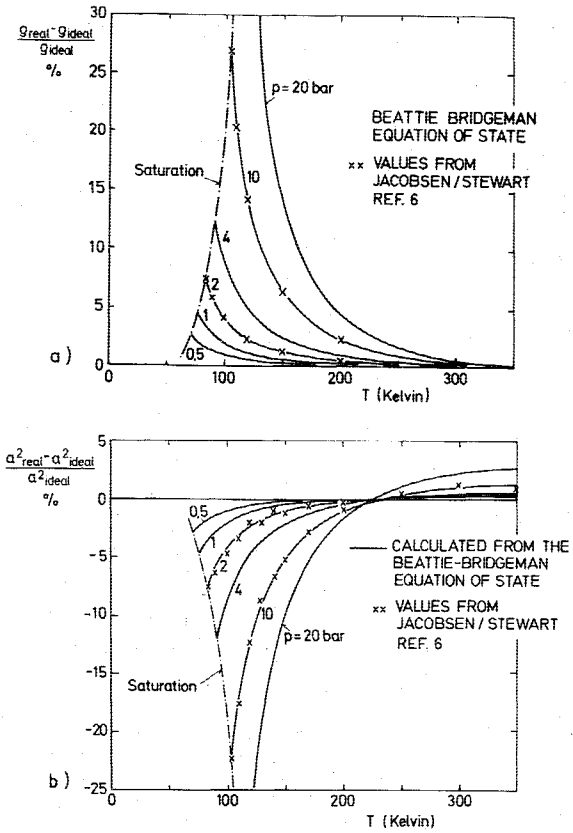

Fig. 1 Deviations of a) the thermal equation of state and b) the speed of sound for real nitrogen from the ideal case.

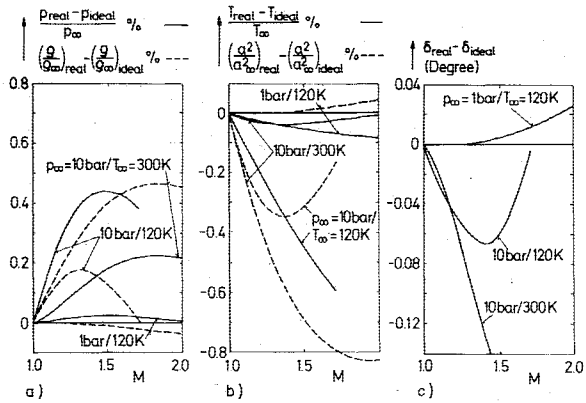

Fig. 2 Prandtl-Meyer expansions in real nitrogen, $M_\infty = 1$.

pressures ($p_\infty = 1$ bar), even in the cryogenic range, the deviations are very small and almost of the same order as at normal temperatures ($T_\infty = 300$ K) and the same pressure. On the other hand, the larger deviations at higher pressures ($p_\infty = 10$ bar) are not restricted to the cryogenic range of temperatures, but are of the same order of magnitude at normal temperatures ($T_\infty = 300$ K). Similar conclusions can be drawn for the deviations shown in Fig. 2b for the temperature and speed-of-sound ratios. The only exception is that for $p_\infty = 10$ bar, $T_\infty = 300$ K, the deviation in the temperature ratio turns out to be the smallest, while the deviation in the ratio of the square of the speed of sound has its largest value. It should be kept in mind that the absolute deviations of density and speed of sound may be larger due to deviations in the initial state of the flow itself. Therefore, it can be important to use real gas equations for determining the operating conditions of cryogenic wind tunnels and for evaluating the experimental data of such tunnels. Figure 2c indicates the deviations in streamline deflection angle δ. For

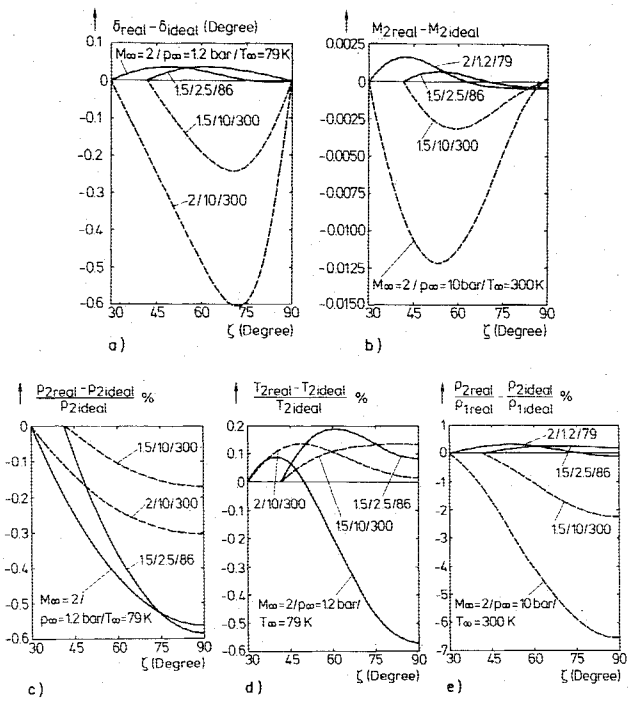

Fig. 3 Oblique shock waves in real nitrogen.

the cryogenic cases they always are smaller than ± 0.1 deg, while for $p_\infty = 10$ bar, $T_\infty = 300$ K, the deviations increase up to -0.4 deg.

For oblique shock waves, the deviations for the deflection angle δ at given shock angle ζ and Mach number M_∞ are shown in Fig. 3a to increase with the deflection angle itself. With increased M_∞ the deviations become larger. At normal temperature $T_\infty = 300$ K they turn out to be a multiple of the deviations in the cryogenic cases with the same initial Mach number. Similar tendencies occur for the deviations in Mach number M_2 behind the shock (Fig. 3b), except the maximal deviation being reached before the maximum in deflection angle. The relative deviations in pressures behind the shock (Fig. 3c) are larger for the cryogenic cases than for 300 K. Such a tendency is also found in Fig. 3d for the static temperature behind the shock. In the cryogenic range, the density ratios differ only by a small amount from the ideal gas behavior in contrast to the ambient temperature cases as shown in Fig. 3e. For estimation of the absolute values of ρ_2 the differences in the initial state between real and ideal gas cases should be considered.

IV. Transonic Small Perturbation Theory

Potential Equation for Small Perturbations

The nonlinear potential equation for steady compressible homentropic flows is valid also for real gases due to its derivation from continuity equation, Euler equations, and constancy of the entropy. Restricting ourselves to flows close to the sonic speed with small perturbations of the flowfield, this equation can be simplified and rewritten for the disturbance potential ϕ. First of all, a series expansion for the local speed of sound is needed (this was done in Ref. 8 in a similar form)

$$a^2 - a_\infty^2 = \left(\frac{\partial (a^2)}{\partial h}\right)_{s,\infty} (h - h_\infty) + \frac{1}{2}\left(\frac{\partial^2 (a^2)}{\partial h^2}\right)_{s,\infty} (h - h_\infty)^2 + \ldots \qquad (16)$$

where the differences in enthalpy can be replaced by the squares of the velocities using the energy equation (14).

Neglecting all terms of the second or higher order in the disturbance velocities, we get for the local speed of sound

$$\frac{a^2}{a_\infty^2} \approx 1 - \left(\frac{\partial a^2}{\partial h}\right)_{s,\infty} M_\infty^2 \frac{u}{V_\infty}$$

u being the disturbance velocity ϕ_x in x direction. Assuming that the squares of the velocity perturbation can be neglected and the cross derivatives are sufficiently small, the potential equation can be simplified to a small perturbation form for the disturbance potential ϕ

$$\{(1-M_\infty^2) - M_\infty^2[2+(\gamma_\infty^*-1)M_\infty^2]\phi_x\}\phi_{xx} + \phi_{yy} + \phi_{zz} = 0 \quad (17a)$$

with the abbreviation

$$\gamma_\infty^* = 1 + \left(\frac{\partial a^2}{\partial h}\right)_{s,\infty} \quad (18)$$

which reduces to the ratio of specific heats γ in the case of ideal gas and makes Eq. (17a) comparable with the form given in Ref. 9.

In general, a slightly different form is used as a potential equation for transonic small perturbations, which can be written in conservation form

$$\{(1-M_\infty^2)\phi_x - [(\gamma_\infty^*+1)/2]M_\infty^2\phi_x^2\}_x + \phi_{yy} + \phi_{zz} = 0 \quad (17b)$$

The calculations for real gas shown in this chapter are performed by solving Eq. (17b) by means of the Dornier relaxation method.

Eqs. (17) and (18) represent the correct first-order potential approximation for transonic flow in real gases. The small perturbation theory cannot account for local changes of γ^*, but its range of validity may be further restricted by such effects in comparison with the ideal gas case.

Pressure Coefficient

A general derivation is presented as a series expansion for pressure coefficients of an isentropic flow in real gas

$$c_p = \frac{p-p_\infty}{q_\infty} = \frac{1}{q_\infty}\left(\frac{\partial p}{\partial V^2}\right)_{s,\infty}(V^2 - V_\infty^2) + \frac{1}{2q_\infty}\left(\frac{\partial^2 p}{\partial (V^2)^2}\right)_{s,\infty}(V^2 - V_\infty^2)^2 + \ldots \quad (19)$$

Using the conservation of energy for an adiabatic flow [Eq. (14)], the first derivative in Eq. (19) can be written

$$\left(\frac{\partial p}{\partial V^2}\right)_s = \left(\frac{\partial p}{\partial h}\right)_s \frac{\partial h}{\partial V^2} = -\frac{1}{2}\left(\frac{\partial p}{\partial h}\right)_s = -\frac{\rho}{2} \quad (20)$$

where the last form is yielded with the aid of the total differential

$$dh = T\,ds + v\,dp \quad (21)$$

The second derivative in Eq. (19) can be found by another differentiation of Eq. (20), at constant entropy, in combination with Eq. (12)

$$\left(\frac{\partial^2 p}{\partial (V^2)^2}\right)_s = \frac{1}{4}\frac{\rho}{(\partial p/\partial \rho)_s} = \frac{1}{4}\frac{\rho}{a^2} \quad (22)$$

Introducing Eq. (22) in Eq. (19) and truncating the series expansion after the second-order terms in the disturbance velocities, the pressure coefficient can be written

$$c_p \approx -2\frac{u}{u_\infty} - \frac{(1-M_\infty^2)u^2 + v^2 + w^2}{U_\infty^2} \quad (23)$$

The result agrees with the usual and well-known form [10] which is proven to be correct for real gas, too. Generally, it should be kept in mind that in transonic flows, terms of u^3 can be of the same order of magnitude as terms in v^2.[9] Continuing the series expansion to terms of the third order, γ_∞^* [Eq. (18)] replaces the specific heat ratio γ within the usual series expansion for ideal gas.

Critical Mach Number, Critical Pressure Coefficient

If the series expansion [Eq. (16)] is terminated behind the first term and the change in enthalpy is replaced by the corresponding velocity differences, the local speed of sound is estimated by

$$\frac{a^2}{a_\infty^2} = \frac{a^2}{V_\infty^2}M_\infty^2 = 1 + \frac{\gamma_\infty^*-1}{2}M_\infty^2\left(1 - \frac{V^2}{V_\infty^2}\right)$$

For critical flow conditions ($a^2 = V^2$) the velocity terms can be replaced by the pressure coefficient [Eq. (23)], restricting all relations to linear terms in disturbance velocities. Resolving for the critical pressure coefficient yields as a first-order approximation

$$c_p^* = -\frac{2}{\gamma_\infty^*+1}\frac{1-M_\infty^2}{M_\infty^2} \quad (24)$$

and for the critical freestream Mach number

$$M_\infty^{*2} = \left(1 - \frac{\gamma_\infty^*+1}{2}c_{p_{\min}}\right)^{-1} \quad (25)$$

if $c_{p_{\min}}$ is the lowest pressure coefficient occurring at the body. Eqs. (24) and (25) totally agree with the approximations for ideal gas [11] if γ^* is replaced by γ.

γ^* and α from the Equations of State

The differential expression $(\partial a^2/\partial h)_s$ which defines γ^* can be evaluated from the equations of state since a^2 is also a thermodynamic property. Assuming $a^2 = a^2(\rho, T)$, $h = h(\rho, T)$, $s = s(\rho, T)$, we get from the corresponding total differentials with the entropy being constant

$$\left(\frac{\partial a^2}{\partial h}\right)_s = \frac{\left(\frac{\partial a^2}{\partial \rho}\right)_T\left(\frac{\partial s}{\partial T}\right)_\rho - \left(\frac{\partial a^2}{\partial T}\right)_\rho\left(\frac{\partial s}{\partial \rho}\right)_T}{\left(\frac{\partial h}{\partial \rho}\right)_T\left(\frac{\partial s}{\partial T}\right)_\rho - \left(\frac{\partial h}{\partial T}\right)_\rho\left(\frac{\partial s}{\partial \rho}\right)_T} \quad (26)$$

The derivatives of the entropy are given by Eqs. (4) and the derivatives of the enthalpy and the speed of sound can be calculated from Eqs. (7) and (12), respectively.

The local adiabatic exponent is defined for a differential change in state by [12]

$$\alpha = -\frac{v}{p}\left(\frac{\partial p}{\partial v}\right)_s = \frac{\rho}{p}a^2 \quad (27)$$

In Ref. 2, it was assumed that accurate real gas flow solutions would result from the use of the effective value of the expansion coefficient α in the ideal gas equations in place of the specific heat ratio. The present study indicates the importance of a further parameter, namely γ^*, which in some cases also has to be used for replacing the ideal value γ. Obviously, this quantity γ^* is more significant in describing the behavior of transonic real gas flows with small perturbations. In the course of flows with large perturbations, both quantities may change quite remarkably.

Results

In Fig. 4a, the computed values of γ^* are plotted against static pressure and static temperature. This figure clearly

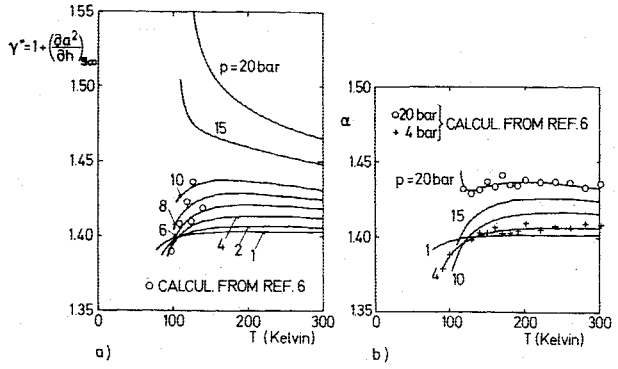

Fig. 4 Coefficients for small perturbation theory in real nitrogen: a) γ^* for transonic flow, b) adiabatic expansion exponent α.

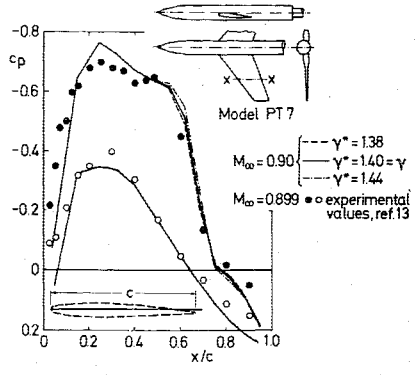

Fig. 5 Small perturbation theory results for a wing section of the wing-body combination PT7, $A = 4$, $\lambda = 0.4$, $\alpha = -1$ deg.

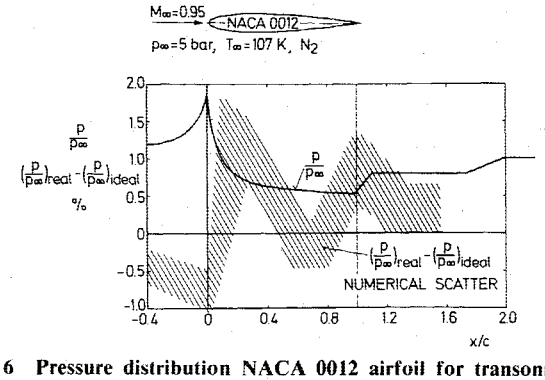

Fig. 6 Pressure distribution NACA 0012 airfoil for transonic inviscid flow in real nitrogen.

indicates that the changes in γ^* are mainly caused by pressure changes and increase with pressure. The temperature influence is comparatively small. For reasonably high pressures up to 10 bar, γ^* is even found to be close to the ideal value of 1.4. For higher pressures, the deviations increase considerably, but the transonic operating range of planned cryogenic wind tunnels does not exceed static pressures of about 5 bar.

For comparison purposes, Fig. 4b presents the corresponding plots for the parameter α calculated from Eqs. (27) and (12). α shows even less deviation from the ideal value of 1.4. Up to $p = 15$ bar, α has a decreasing tendency with decreasing temperature. In addition, from Figs. 4a and b, some values for γ^* and α are shown, as derived directly from the data of Ref. 6. They generally show good agreement, the scatter of the α data being due to the round-off errors in the speed of sound values in Ref. 6.

Figure 5 shows the results for a three-dimensional transonic small perturbation calculation for real nitrogen. Besides the ideal value $\gamma = 1.4$, the values $\gamma^*_\infty = 1.38$ and $\gamma^*_\infty = 1.44$ were used which cover a pressure region of more than the whole cryogenic range of interest, as shown in Fig. 4a. The computations were done for the wing-body combination PT7 using the conservative Dornier relaxation method.[13] The c_p distributions show only small influences of γ^*_∞. They mainly cause changes in the shock position which are of the order of accuracy of the computational method. The computations were performed without boundary-layer corrections and represent fully converged solutions.

V. Inviscid Rotational Flows

To study the real gas effects in transonic flow without any limitation to weak shocks or isentropic flow, the flowfield around an aerofoil is studied by means of the numerical solution of the full two-dimensional inviscid equations. The finite volume technique is used as a numerical method due to its conservation of mass, momentum, and energy which is formulated in a quite general form without any restrictions as far as the equations of state are concerned. The equations of state in the method for an ideal gas are easily replaced by those equations presented in Sec. II. The program is solving the time-dependent equations which reach the steady-state with time.

The time-dependent conservation equations without volume-forces can be written in integral form for an arbitrary surface fixed in space

$$\frac{\partial}{\partial t}\iint_S U\,\mathrm{d}s + \oint_C \bar{\bar{H}}(U)\cdot \mathrm{d}c = 0 \tag{28a}$$

where S is the surface element, C its circumference, U the vector

$$U = \begin{Bmatrix} \rho \\ \rho u \\ \rho v \\ \rho[e + \tfrac{1}{2}(u^2+v^2)] \end{Bmatrix} \tag{28b}$$

and $\bar{\bar{H}}(U)$ the flux tensor

$$\bar{\bar{H}}(U) = \begin{Bmatrix} \rho V \\ \rho u V + p i_x \\ \rho v V + p i_y \\ [\rho(e + \tfrac{1}{2}V^2) + p]V \end{Bmatrix} \tag{28c}$$

This forms a set of four scalar nonlinear equations for the five unknowns u,v,ρ,p, and e. This system can be solved if, in addition, a thermodynamic relation is used which connects the flow properties ρ,p, and e. Such an expression is formulated by the equations for real gases [Eqs. (1) and (6)]. From these equations, p can be calculated iteratively via the temperature if ρ and e are known.

The numerical procedure is very similar to the finite-volume method of Rizzi.[14] A detailed description of the present method is given in Ref. 15.

In Fig. 6, the results from the finite-volume method are plotted for the NACA 0012 aerofoil at 0 deg angle of attack and Mach number $M_\infty = 0.95$. In spite of noticeable numerical scatter, some small systematic deviations occur for the cryogenic nitrogen, compared with the results for an ideal diatomic gas ($\gamma = 1.4$). The differences between both cases exhibit a relative maximum at the stagnation point and a zero at $p/p_\infty = 1$. Apparently, the oblique trailing edge shock for the real gas flow is located within a very short distance upstream of its position in the ideal case. The position of the normal shock occurring further downstream is not calculated

accurately enough to correctly predict the corresponding real gas influences.

VI. Shock-Wave/Boundary-Layer Interaction

To judge the real gas influence for viscous transonic flows, the interaction between an oblique shock wave and a laminar boundary layer was studied for real gas as well as the ideal one. This flow problem was chosen due to the relatively simple geometry and especially because of the experimental results for ideal gas being available. A laminar boundary layer ($Re \approx 3 \cdot 10^5$) was used not to get involved with turbulence models, although the computational method used is capable of treating turbulent flows at high Reynolds numbers.

The conservation equations to be solved now are the full two-dimensional time-dependent laminar compressible Navier-Stokes equations. They can be written in the same form as Eq. (28a), U being defined identically as in Eq. (28b). In contrast to Eq. (28c) the tensor $\bar{\bar{H}}$ has to now include the viscous terms and the heat flux components

$$\bar{\bar{H}}(U) = \begin{Bmatrix} \rho V \\ \rho u V - \bar{\bar{T}} \cdot i_x \\ \rho v V - \bar{\bar{T}} \cdot i_y \\ [\rho (e + V^2/2) - \bar{\bar{T}}] \cdot V + q \end{Bmatrix} \tag{29a}$$

$\bar{\bar{T}}$ being the stress tensor, and q the heat flux vector. The stresses can be written for laminar flows

$$\bar{\bar{T}} = 2\eta \bar{\bar{D}} - (p + \tfrac{2}{3}\eta \operatorname{div} V)\bar{\bar{E}} \tag{29b}$$

with $\bar{\bar{D}}$ as deformation tensor and $\bar{\bar{E}}$ as unity tensor.

The shear viscosity η is taken from the Sutherland formula

$$\eta = B \frac{\sqrt{T}}{1 + C/T} \tag{30a}$$

The constants B, C are given in Ref. 16 as

$$B = 1.378 \times 10^{-6} \qquad C = 103 \tag{30b}$$

for T in K and η in kg/(m-s). Though the constants originally are valid for a different range of temperatures,[16] the comparison with the experimental values for η from Ref. 17, as shown in Fig. 7, show good agreement even in the range of cryogenic temperatures. The heat flux is defined by Fourier's law

$$q = -k \operatorname{grad} T \tag{31}$$

For ideal gases, the heat conductivity k is usually calculated from the viscosity under the assumption of constant Prandtl number

$$Pr = c_p \eta / k \tag{32}$$

At cryogenic temperatures, the Prandtl number is not constant (see, for example Ref. 5 or Fig. 7) and such a procedure is not allowed. Instead, a formula for k will be defined similar to the Sutherland representation for η

$$k = D \frac{\sqrt{T}}{1 + E/T} \tag{33a}$$

The constants D and E are estimated in comparison with the experimental data for k in Ref. 17 within the temperature range $80\,K < T < 300$ K for nitrogen

$$D = 2.067 \times 10^{-3} \qquad E = 111 \tag{33b}$$

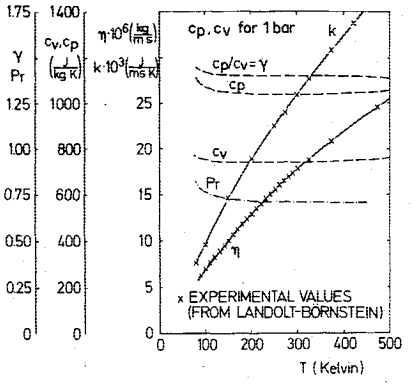

Fig. 7 Material properties for nitrogen.

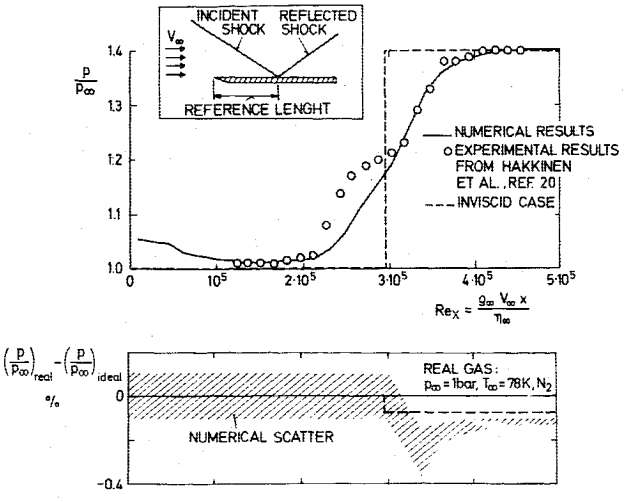

Fig. 8 Pressure distribution for shock-wave/boundary-layer interaction, $Re = 2.96 \times 10^5$, $M_\infty = 2$, $\zeta = 32.585$ deg.

T being given in K and k in J/(m-s-K). The constants C in Eq. (30b) and E in Eq. (33b) have different values. Therefore, the ratio of η and k is not exactly constant as it is true for ideal gas. As proved by the experimental data in Ref. 17, the dependence of η and k on pressure can be neglected in the whole range of temperatures, if the pressures are restricted to the levels considered for cryogenic wind tunnels.

When Eqs. (29-33) are introduced in Eq. (28), four equations remain for the six unknowns u, v, ρ, p, e, and T. To end up with a set of equations that can be solved, the thermodynamic equations of state [Eqs. (1) and (6)] have to be used to connect ρ, p, e, and T.

The numerical solution of the set of equations [Eq. (28)] is done by means of MacCormack's finite-volume/time-splitting approach.[18,19] The procedure is very similar to the finite-volume approach to solve the inviscid equations of Sec V. Due to the viscous stress and heat conduction terms, still derivatives of velocities u, v and of temperature T remain. These derivatives have to be calculated by means of a simple finite difference scheme.

As an example for the numerical computation, the laminar shock-wave/boundary-layer interaction, as studied experimentally by Hakkinen et al.[20] and computed by MacCormack[18,19] for an ideal gas, was taken. The special case chosen was that with a freestream Mach number $M_\infty = 2.0$, a shock angle for the incident shock $\zeta = 32.585$ deg, and a Reynolds number for the flat plate at the shock foot $Re = 2.96 \times 10^5$. These conditions have been held constant for real and ideal gas cases and correspond to a pressure ratio of about 1.4 between the freestream pressure and the pressure behind the reflected shock. For this case exists a small, shock-induced separation region.

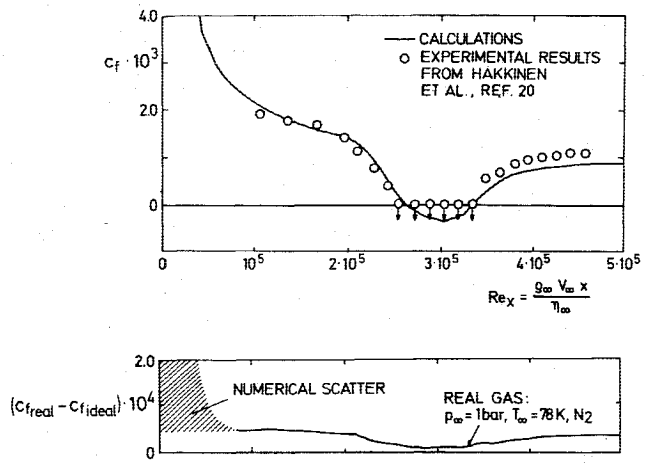

Fig. 9 Distribution of wall shear stress for shock-wave/boundary-layer interaction, $Re = 2.96 \times 10^5$, $M_\infty = 2$, $\zeta = 32.585$ deg.

The upstream conditions for pressure and temperature for the ideal gas case correspond to those of the experiment.[20] The numerical results for this case are in good agreement with the experiments as shown in Figs. 8 and 9 for the pressures at the wall as well as for the shear stresses. The separation point and the reattachment point are well predicted. The differences between the theoretical and experimental pressure distribution within the separation bubble could be reduced by a mesh refinement.[21]

The upstream conditions for the real gas case correspond to a point on the vapor pressure curve with 1 bar static pressure. The wall pressure deviations of the real gas case from the ideal one are within the range of numerical scatter upstream of the shock impingement. Downstream of the shock wave, these results show systematic deviations close to those of the inviscid outer flow. Therefore, concerning the pressure distribution, real gas effects seem to be impressed on the boundary layer by the outer flow, and then are plausible from boundary-layer theory. However, the wall shear stress distribution exhibits small systematic deviations from the ideal gas case along the whole flat plate length which differ in sign for both bases. These effects can be shown to be due to two basic facts which tend to alleviate each other.[22] First, the boundary-layer temperatures are diminished in consequence of the caloric imperfections of the real gas, while the profiles of the internal energy remain nearly unchanged. Because of Eq. (30), this tends to reduce the viscosity at the wall. Secondly, the slope of the viscosity curve steepens with decreasing temperature (see Fig. 7) which counteracts the first effect. The second one is dominant in the real gas case of Fig. 9. Since the influence on the dimensionless velocity profiles also remain very small, the deviations in the skin friction can be explained in this manner with respect to sign as well as magnitude.

VII. Conclusions

The present results prove the real gas effects to remain small in the operating range considered for cryogenic wind tunnels. The deviations are mainly due to pressure and due less to temperature influence. In some cases, they are definitely higher at ambient temperatures. The coefficient γ^* for small perturbation theory characterizes the dependence of the real gas effects on pressure and temperature in a typical manner. In viscous flows, some systematic changes in skin friction occur caused by a temperature variation due to the caloric imperfections and by a change of the viscosity characteristics with decreasing temperature.

More detailed information concerning the present work can be found in Refs. 22 and 23.

References

[1] Howell, R. R. and McKinney, W., "The U.S. 2.5 Meter Cryogenic High Reynolds Number Transonic Tunnel," ICAS Paper 76-04, 10th ICAS Congress, Ottawa, Canada, 1976.

[2] Adcock, J. B., Kilgore, R. A., and Ray, E. J., "Cryogenic Nitrogen as a Transonic Wind Tunnel Test Gas," AIAA Paper 75-143, Pasadena, Calif., 1975.

[3] Landolt-Börnstein, *Zahlenwerte und Funktionen*, IV. Band, 4. Teil, Bandteil a, herausgegeben von H. Hausen, Springer-Verlag, Berlin/Heidelberg/New York, 6. Auflage, 1967.

[4] Baehr, H. D., *Thermodynamik*, Springer-Verlag, Berlin/Heidelberg/New York, 2. Auflage, 1966.

[5] Becker, E., *Gasdynamik*, B. G. Teubner Verlagsgesellschaft, Stuttgart, 1966.

[6] Jacobsen, R. T. and Stewart, R. B., "Thermodynamic Properties of Nitrogen Including Liquid and Vapor Phases from 63 K to 2000 K With Pressures to 10.000 bar, *Journal of Chemical Physics Reference Data*, Vol. 2, 1973, pp. 757-922.

[7] Woolley, H. W. and Benedict, W. S., "Generalized Tables of Corrections to Thermodynamic Properties for Nonpolar Gases," NACA TN 3272, 1956.

[8] ONERA, private communication, 1976.

[9] Zierep, J., *Theoretische Gasdynamik 2-Schallnahe und Hyperschallströmungen*, Verlag G. Braun, Karlsruhe, 1966 and 1972.

[10] Shapiro, A. H., *The Dynamics and Thermodynamics of Compressible Fluid Flow*, The Ronald Press Company, New York, 1953.

[11] Schlichting, H. and Truckenbrodt, E., *Aerodynamik des Flugzeugs I*, Springer-Verlag, Berlin/Heidelberg/New York, 2. Auflage, 1967.

[12] Iberall, A., "The Effective Gamma for Isentropic Expansions of Real Gases," *Journal of Applied Physics*, Vol. 19, 1948, pp. 997-999.

[13] Schmidt, W. and Hedman, S., "Recent Explorations in Relaxation Methods for Three-Dimensional Transonic Potential Flow," ICAS Paper 76-22, 1976.

[14] Rizzi, A., "Transonic Solutions of the Euler Equations by the Finite Volume Method," *Symposium Transsonicum II*, Springer-Verlag, Heidelberg/Berlin/New York, 1976.

[15] Lucci, C. W., Schmidt, W., and Tambach, T., "Berechnungsverfahren für reibungsfreie Transsonische Strömungen, Dornier-FB 76/55 B, 1976.

[16] Landolt-Börnstein, *Zahlenwerte und Funktionen*, IV. Band, 1. Teil, herausgegeben von E. Schmidt, Springer-Verlag, Berlin/Göttingen/Heidelberg, 6. Auflage, 1955.

[17] Landolt-Börnstein, *Zahlenwerte und Funktionen*, II. Band, 5. Teil, herausgegeben von K. Schäfer, Springer-Verlag, Berlin/Heidelberg/New York, 6. Auflage, 1968/69.

[18] MacCormack, R. W., "Numerical Solution of the Interaction of a Shock Wave with a Laminar Boundary Layer," *Lecture Notes in Physics*, Vol. 8, Springer-Verlag, Berlin/Heidelberg/New York, 1971, pp. 151-163.

[19] MacCormack, R. W., "Numerical Methods for Hyperbolic Systems," Short Course on Advances in Computational Fluid Dynamics, Tullahoma, Tenn., Dec. 10-14, 1973.

[20] Hakkinen, R. J., Greber, I., Trilling, L., and Abarbanel, S. S., "The Interaction of an Oblique Shock Wave with a Laminar Boundary Layer," NASA Memo. 2-18-59 W, 1959.

[21] Murphy, J. D., Presley, L. L., and Rose, W. C., "On the Calculation of Supersonic Separating and Reattaching Flows," AGARD-CP-198, 1975.

[22] Wagner, B. and Schmidt, W., "Theoretische Untersuchungen zur Stoß-Grenzschicht-Wechselwirkung in kryogenem Stickstoff," to be published in *Zeitschrift für Flugwissenschaften und Weltraumforschung* (*ZFW*), 1978.

[23] Wagner, B. and Schmidt, W., "Theoretical Investigations of Real Gas Effects in Cryogenic Wind Tunnels," Dornier FB 76/50 B, 1976.